www.czasopisma.pan.pl PAN www.journals.pan.pl

ARCHIVES of FOUNDRY ENGINEERING

DE GRUYTER OPEN

ISSN (2299-2944)
Volume 15
Issue 4/2015

DOI: 10.1515/afe-2015-0088

Published quarterly as the organ of the Foundry Commission of the Polish Academy of Sciences

101 – 109

Thermodynamic Assessment of Mushy Zone in Directional Solidification

P. Mikołajczak*[a], L. Ratke[b]

[a] Institute of Materials Technology, Poznan University of Technology, Piotrowo 3, 60-965 Poznan, Poland
[b] Institut für Werkstoff-Forschung, German Aerospace Center DLR,
Linder Höhe, 51147 Köln, Germany
*Corresponding author. E-mail address: Piotr.Mikolajczak@put.poznan.pl

Received 19.06.2015; accepted in revised form 15.07.2015

Abstract

Solidification of AlSiFe alloys was studied using a directional solidification facility and the CALPHAD technique was applied to calculate phase diagrams and to predict occurring phases. The specimens solidified by electromagnetic stirring showed segregation across, and the measured chemical compositions were transferred into phase diagrams. The ternary phase diagrams presented different solidification paths caused by segregation in each selected specimen. The property diagrams showed modification in the sequence and precipitation temperature of the phases. It is proposed in the study to use thermodynamic calculations with Thermo-Calc which enables us to visualize the mushy zone in directional solidification. 2D maps based on property diagrams show a mushy zone with a liquid channel in the AlSi7Fe1.0 specimen center, where significant mass fraction (33%) of β-Al_5FeSi phases may precipitate before α-Al dendrites form. Otherwise liquid channel occurred almost empty of β in AlSi7Fe0.5 specimen and completely without β in AlSi9Fe0.2. The property diagrams revealed also possible formation of α–Al_8Fe_2Si phases.

Keywords: Aluminum alloys, Directional solidification, Mushy zone, CALPHAD, Fe intermetallics, β-Al_5FeSi

1. Introduction

The design of industrial processes requires understanding of the relationship between composition, microstructure and process conditions. In materials science, the complex correlations can be described as phase diagrams, for simple and complicated materials systems. The equilibrium phase diagram mainly presents the regions where substances or phases are stable and two or more of them coexist. The very extensive study of phase diagrams was presented by Massalski [1]. The modern technique CALPHAD (CALculation of PHAse Diagrams) can be applied to model thermodynamic properties of occurring phases and to predict behavior and interactions between phases [2,3]. The CALPHAD [3,4,5] method requires data bases with theoretical and experimentally received information about phases equilibria and thermomechanical properties in a studied system. The interrelations between phases and each phase are modeled with the Gibbs free energy, using mathematical modeling aided by some parameters [3,4,5]. It is not possible to receive a precise description of the values of the Gibbs energy of a complex system with analytical equations. The parameters for phases description or the relationship are gained by fitting the model to existing information. After collecting data bases, models and parameters, it is possible to calculate the phase diagram especially in regions without experimental data or for metastable states and for multi-component system [3,4,5].

Cast aluminum alloys are cost-effective materials due to the low melting point and high strength. The most important cast aluminum alloy system is Al–Si, where silicon (4.0–13%) contribute to give good casting properties. Aluminum alloys are widely used in engineering structures and components where light

weight or corrosion resistance is required, especially in automotive industry. Alloys composed mostly of aluminum have been very important in aircraft and aerospace manufacturing and still competitive to plastic composites. The microstructure of AlSi alloys consist of α-Al dendrites, Al-Si eutectic and other phases by presence of Mn, Fe, Mg, Cu and other elements. Aluminum alloys with even small amounts of iron causes formation of intermediate Fe-rich phases like the deleterious monoclinic β-Al_5FeSi (Fig. 1 and 2, for interpretation of the references to color in all figures legend, the reader is referred to the web version of this article).

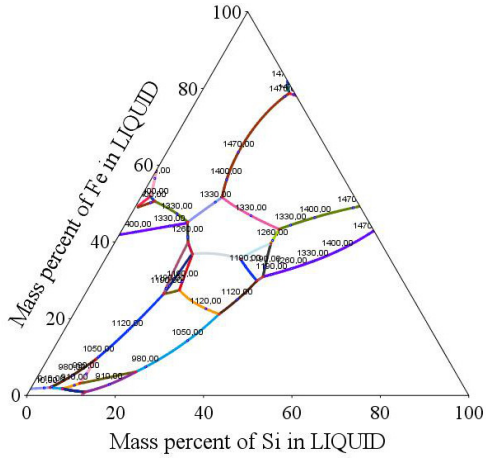

Fig. 1a. Ternary phase diagram – Al-Si-Fe system

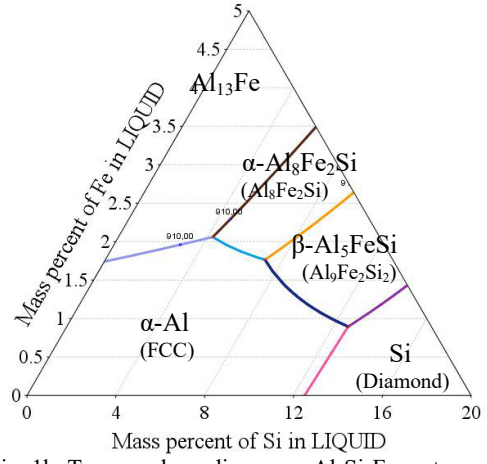

Fig. 1b. Ternary phase diagram – Al-Si-Fe system – Liquidus projection of Al rich corner

One of the important research techniques is directional solidification technology. The directional solidification allows to control cooling rate and temperature gradient in broad range inside the solidifying directionally specimens and to study interface evolution, solute redistribution, phase selection and crystal growth instability [6,7]. Well known are instruments of Czochralski [8], Bridgman-Stockbarger [9] and Chalmers. One of the methods for conduction of directional solidification is the aerogel based power down method that uses two controlled heaters [10,11,12].

In the current paper we applied the thermodynamic calculations for estimation of the mushy zone and prediction of phases precipitation in directional solidification [10,12] experiments of AlSi alloys with Fe-rich intermetallics. The software package Thermo-Calc [13] was used for calculation of ternary phase diagrams, Scheil solidification and property diagrams and to create 2D maps of the mushy zone.

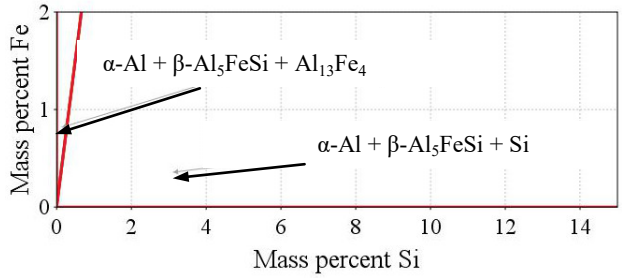

Fig. 2. Ternary phase diagram – Al-Si-Fe system – Isothermal section at 20 ºC

2. Methodology

For the studied alloys and their properties we have applied Thermo-Calc 4.1 [13] software (using the CALPHAD approach) with TCAl3 (TCS Al-based alloys database v.3) and MOBAl3 (TCS Al-alloys mobility database v.3) databases. Thermo-Calc can be used for a wide variety of applications like calculation of: stable and meta-stable heterogeneous phase equilibria, amounts of phases and their compositions as a function of temperature and chemistry, phase transformation temperatures, such as liquidus, solidus, phase diagrams, binary, ternary and isoplethal and isothermal sections for higher order systems, thermochemical data such as enthalpies, heat capacity and activities, driving force for phase transformations, solidification applying the Scheil-Gulliver model.

For the study we made use of the part of the experimental results [14,15] for aluminum alloys with 5, 7 and 9 wt.% Si and 0.2, 0.5 and 1.0 wt.% Fe prepared from pure components: Al (99.999% Hydro Aluminum Deutschland GmbH), Si (Crystal Growth Laboratory, Berlin, Germany) and Fe from ferroaluminum (50 wt.% Al-50 wt.% Fe, Goodfellow Cambridge Ltd, UK) [14]. Specimens with 8 mm diameter and 120 length were processed in Artemis-3 facility, which allows directional solidification of metal alloys under controlled conditions [10,11,12]. The cylindrical specimens were solidified directionally upwards with a temperature gradient G = 3 K/mm and solidification velocity v = 0.04 mm/s, with fluid flow induced inside the specimen by a rotating magnetic field (RMF) with induction B = 6 mT at a frequency of 50 Hz, inducing first azimuthal flow and additionally secondary flows in radial and axial directions [14,15]. The solidified samples were cut (Isocut 4000, Buehler) at a height of 45 mm (for longitudinal section, Fig. 3) from the bottom heater. The composition on the specimen sections (Fig. 4) was investigated with EDX (Oxford INCA System) [14].

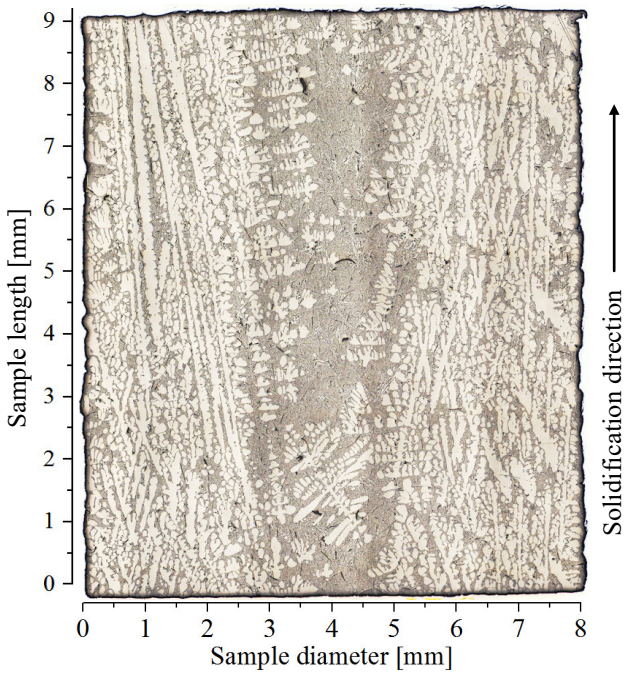

Fig. 3. A microstructure on the longitudinal section of the Al-7wt.%Si-1.0wt.%Fe specimen solidified under influence of a rotating magnetic field (G = 3 K/mm, v = 0.04 mm/s, B = 6 mT)

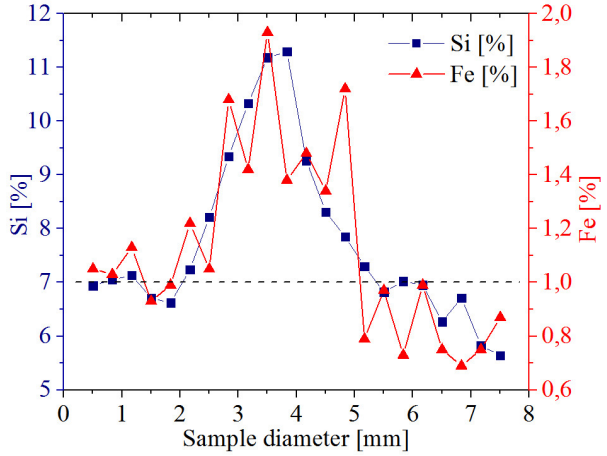

Fig. 4. Si and Fe concentration profile on the Al-7wt.%Si-1.0wt.%Fe specimen (G = 3 K/mm, v = 0.04 mm/s, B = 6 mT) measured on cross section in 22 points (distance 0.333 mm)

In the current study, we selected and made use of the four specimens, with composition AlSi5Fe1.0, AlSi7Fe1.0, AlS7Fe0.5 and AlSi9Fe0.2 solidified only with induced flow (with RMF). The measurement of the chemical composition presented the segregation on the cross-section [14] (Fig. 4) that was also visible on the longitudinal section as increase in eutectic fraction (Fig. 3). The measured chemical compositions were presented on the ternary phase diagram Al-Si-Fe and were treated as potentially solidifying alloys in the specimens. For selected extreme compositions, the solidification paths with Scheil Solidification (Scheil-Gulliver) in Thermo-Calc was calculated, to make possible analyzing the different solidification manner.

For selected chemical compositions (measurement points on the section) the Property Diagrams in Thermo-Calc were calculated, for presentation of the precipitation sequence and fraction of solidified phases, e.g. for AlSi5Fe1.0 specimen, the compositions AlSi6.63Fe1.71 and AlSi5.09Fe0.57 were analyzed. The chemical composition was chosen adequately to present the extreme possible solidification manner and was visualized as property diagrams (mass fraction of the phases as function of temperature). For all specimens and measured compositions (in all 22 measurement points on cross-section, with distance between 0.333 mm, Fig. 4), the Property Diagrams were calculated. For each specimen, the Property Diagrams were collected to prepare 2D maps showing mass fraction (of Liquid, α-Al, β-Al_5FeSi) as function of location on the longitudinal section and temperature of phases precipitation. The controlled solidification condition (temperature gradient, velocity, cooling rate) in Artemis-3 allowed for rescaling the temperature axis into the length axis, showing in this way 2D maps of mushy zone, as function of location across and along the specimen (solidification direction).

The Ternary Phase Diagram (Fig. 5 and 6) was calculated in Thermo-Calc [13] as Liquidus projection by temperature range 550-900 °C and interval 2 °C. Scheil Solidification was prepared by temperature interval 1 °C and mass fraction interval 0.005. Property Diagrams (Fig. 7-14) were generated by temperature interval 2 °C and mass fraction interval 0.017-0.059 (for Liquid), 0.017-0.059 (for α-Al), 0.00017-0.00148 (for β-Al_5FeSi).

3. Results and Discussion

The specimens with nominal compositions AlSi5Fe1.0, AlSi7Fe1.0, AlSi7Fe0.5 and AlSi9Fe0.2 [14] solidified directionally in Artemis-3 with fluid flow (generated by RMF) were precisely examined. The chemical composition measured on the cross-section was presented on the phase diagram together with selected solidification paths. For selected points on the cross-section the phases precipitation and mushy zone was investigated using property diagrams and created 2D maps.

Considering the mentioned alloys and nominal compositions (AlSi5Fe1.0, AlSi7Fe1.0, AlSi7Fe0.5 and AlSi9Fe0.2) and analyzing the solidification path on the basis of the ternary Al-Fe-Si phase diagram (Fig.1 and 5), we can state, that for AlSi5Fe1.0 specimen (for nominal composition Al-5wt.%Si-1.0wt.%Fe), first α-Al form at the 900.4 K (627.4 ºC) (L → α-Al + L), then sample enriches in Si to a concentration of 7.77 %Si and 1.63 %Fe and reaches the eutectic reaction at 881.4 K (608.4 ºC). Next solidification follow the eutectic groove L → α-Al + β-Al_5FeSi + L starting from 881.4 K (608.4 ºC) and ends at 848 K (575 ºC) where final eutectic reaction L → α-Al + β-Al_5FeSi + Si occurs. For AlSi7Fe1.0 specimen (for nominal composition Al-7wt.%Si-1.0wt.%Fe), α-Al start to form at the 887.7 K (614.7 ºC) (L → α-Al + L), then sample enriches to 9.19 %Si and 1.35 %Fe and reaches the eutectic reaction at 872.5 K (599.5 ºC), and follow the eutectic groove L → α-Al + β-Al_5FeSi + L. Solidification ends at 848 K (575 ºC) with final eutectic reaction L → α-Al + β-Al_5FeSi + Si. For AlSi7Fe0.5 (for nominal composition Al-

7wt.%Si-0.5wt.%Fe), α-Al start to form at the 888.6 K (615.6 ºC) (L → α-Al + L), then sample enriches to 12.26 %Si and 0.94 %Fe and reaches the eutectic reaction at 851.0 K (578.0 ºC), and follow the eutectic groove L → α-Al + β-Al_5FeSi + L to 848 K (575 ºC) with final reaction L → α-Al + β-Al_5FeSi + Si. For AlSi9Fe02 specimen (for nominal composition Al-9wt.%Si-0.2wt.%Fe), first, α-Al forms at 875.5 K (602.5 ºC). On further cooling, the melt enriches up to 12.5 wt.% Si and 0.3 wt.% Fe and reaches the eutectic valley at 849 K (576 ºC), where the AlSi-eutectic form L → α-Al + Si + L, next solidification follows until 848 K (575 ºC), where the final ternary eutectic reaction L → α-Al + β-Al_5FeSi + Si occurs.

Fluid flow generated during solidification caused segregation on the cross-section (Fig. 4) [14]. Chemical compositions (measured with EDX) in distinct points (22 points on the cross section, along sample diameter on Fig. 4) were transferred on the ternary phase diagram AlSiFe (Fig. 5). On the specimen with nominal composition AlSi5Fe1.0 (marked as filled red circle, Fig. 5) the measured compositions (marked as red circles, Fig. 5) are located in the area in that α-Al dendrites form as first phase. Only in one point with chemical composition AlSi9.43Fe1.99 β-Al_5FeSi can precipitate as first phase. On the specimen with nominal alloy composition AlSi7Fe1.0 (filled blue triangle) in 16 from 22 measurement points (marked as blue triangles), α-Al was noticed as first phase to grow, whilst β-Al_5FeSi in other 6 points. On the specimens AlSi7Fe0.5 (green square) and AlSi9Fe0.2 (brown rhombus), in all points α-Al dendrites start to grow as first phase. For selected chemical compositions (measurement points) with extreme content of Si and Fe (in chosen specimen) solidification paths were calculated (Fig. 6) and these differ from mentioned above paths for nominal compositions (AlSi5Fe1.0, AlSi7Fe1.0, AlSi7Fe0.5 and AlSi9Fe0.2) in the specimens.

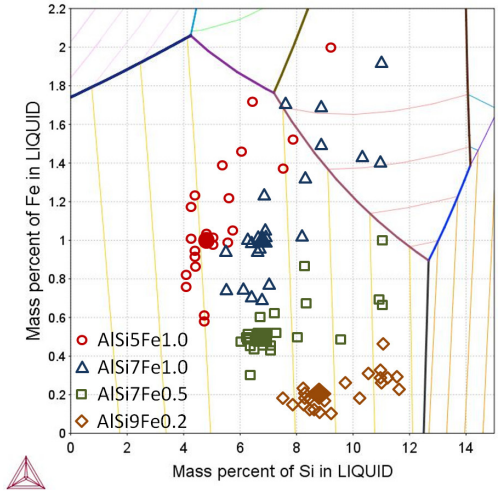

Fig. 5. Ternary phase diagram – Al-Si-Fe system. Liquidus projection with marked chemical compositions measured on the specimens in selected 22 points (as on Fig. 4)

Property diagrams (Fig. 7-10) presenting mass fraction of growing phases in function of the temperature were calculated for chosen compositions (points on the cross-section). It is clear that for the specimen AlSi5Fe1.0 (Fig. 7) there occur places (points) where liquidus temperature can have different value, 628 ºC in point with composition AlSi5.09Fe0.57 and 615 ºC for AlSi6.63Fe1.71. For the composition AlSi6.63Fe1.71 (point with coordinate 4.8 mm) the precipitation of α–Al_8Fe_2Si phase in temperature range 614-612 ºC (Fig. 7) was observed, similarly as for AlSi4.57Fe1.1.7 (point with coordinate 0.5 mm, white ellipse in the Fig. 11) and AlSi4.62Fe1.23 (point with coordinate 5.8 mm), where solidification follow first eutectic groove L → α-Al + α-Al_8Fe_2Si + L and just next L → α-Al + β-Al_5FeSi + L.

For AlSi7Fe1.0 α-Al is the first phase to grow (Fig. 5-6). Property diagram for the point with composition AlSi6.7Fe0.69 (Fig. 8) shows α-Al dendrites starting to grow at the temperature 617 ºC and β-Al_5FeSi just at 590 ºC, whilst for AlSi11.18Fe1.93 first precipitate β-Al_5FeSi at 619 ºC and α-Al at 587 ºC. This indicate that in the place with composition AlSi11.18Fe1.93 (point with coordinate 3,50 mm), α-Al started to grow at 587 ºC while β-Al_5FeSi released largely already with mass fraction 0.0332 (almost half of the whole amount). At the end of eutectic grove L → α-Al + β-Al_5FeSi + L, β-Al_5FeSi mass fraction f_β reached 0.0453 and 0.0700 at 575 ºC with final L → α-Al + β-Al_5FeSi + Si reaction.

In principle, in the whole specimen AlSi7Fe0.5 (Fig. 9), α-Al dendrites grow as first, e.g. at 618 ºC in place with composition AlSi6.57Fe0.33 and at 607 ºC for AlSi8.21Fe0.86. About half of the specimen has composition where β-Al_5FeSi grow as the second phase, e.g. at 590 ºC for AlSi6.57Fe0.33, whilst in the second half AlSi eutectics start as the second at 576 ºC, before the β-Al_5FeSi at 575 ºC.

In the specimen AlSi9Fe0.2 (Fig. 10), as first α-Al dendrites start to grow e.g. at 603 ºC for AlSi9.01Fe0.16 or at 584 ºC for AlSi11.54Fe0.44, and next AlSi eutectics at 577 ºC or 576 ºC respectively, and finally β-Al_5FeSi at 575 ºC.

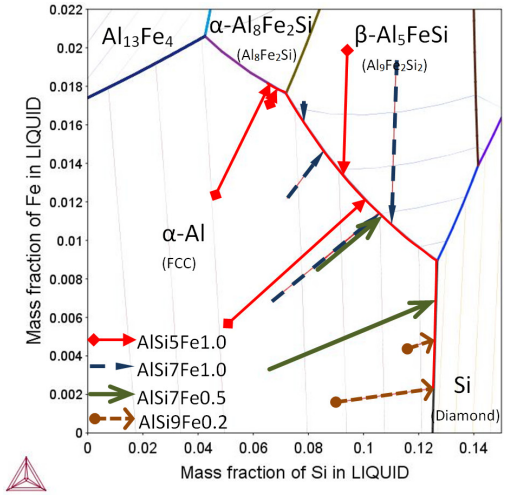

Fig. 6. Ternary phase diagram – Al-Si-Fe system. Liquidus projection with marked solidification paths (Scheil-Gulliver solidification)

Property diagrams calculated for each measured chemical composition (each of 22 points along sample diameter) were located according to the position on the specimen and allowed to create 2D maps (Fig. 11-14) showing mass fraction (of Liquid, α-

Al, β-Al_5FeSi) as function of location on the longitudinal section and temperature of phases precipitation. Controlled solidification in Artemis-3 allowed for rescaling the temperature axis on the length axis, showing in this way 2D maps of mushy zone.

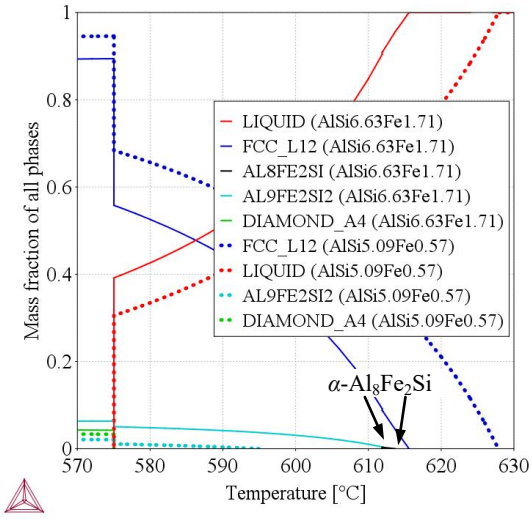

Fig. 7. Property diagram for alloy with chemical composition AlSi6.63Fe1.71 and AlSi5.09Fe0.57

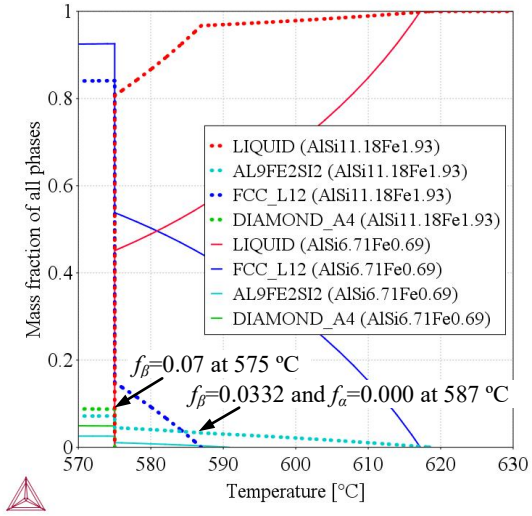

Fig. 8. Property diagram for alloy with chemical composition AlSi11.18Fe1.93 and AlSi6.71Fe0.69

Liquid mass fraction f_L (Fig. 11a) and α-Al mass fraction f_α (Fig. 11b) for specimen AlSi5Fe1.0 clearly show the liquid channel in the specimen center, 0.5 mm wide in the bottom at the temperature 595 ºC and 3 mm on top at 625 ºC. α-Al dendrites start to grow at about 630 ºC in external part of the specimen, and at 595 ºC in the center and the mushy zone seems to be in the temperature range from about 575 ºC to about 630 ºC (Fig. 7, 11), this means about 18 mm long. β-Al_5FeSi (Fig. 11c) start to precipitate in the center at about 600-610 ºC (earlier than outside),

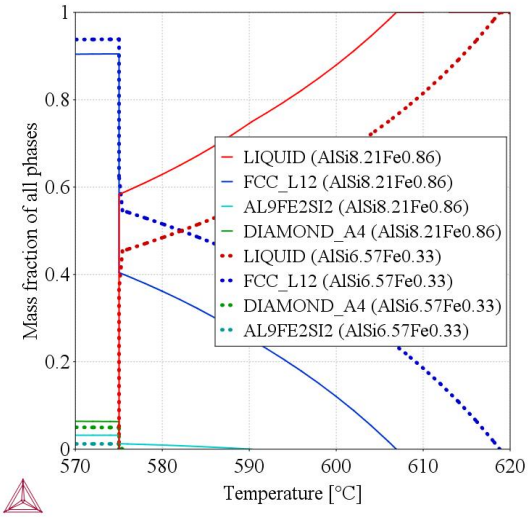

Fig. 9. Property diagram for alloy with chemical composition AlSi8.21Fe0.86 and AlSi6.57Fe0.33

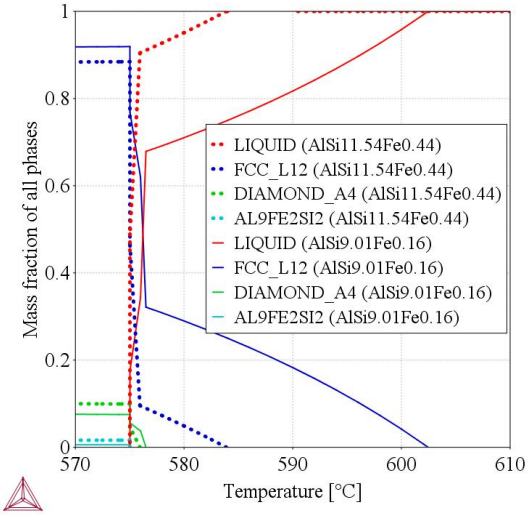

Fig. 10. Property diagram for alloy with chemical composition AlSi8.21Fe0.86 and AlSi6.57Fe0.33

and this corresponds with high Liquid mass fraction (Fig. 11a) and very low α-Al mass fraction (Fig. 11b). The final microstructure solidified at 757 ºC in the center is richer in β-Al_5FeSi (mass fraction about f_β=0.07) and agrees qualitatively with the measurements of number density n_β and length L_β [14] of β-Al_5FeSi phases. Solidification range for β-Al_5FeSi is about 575-610 ºC and e.g. β-Al_5FeSi mass fraction f_β=0.02 reaches the temperature 605 ºC. In one central point on the specimen cross-section with composition AlSi9.43Fe1.99 (Fig. 5-6) β-Al_5FeSi start to grow as first before α-Al dendrites. The liquid channel agrees with central area enriched in β-Al_5FeSi. In the three points with coordinates 0.8 (composition AlSi4.57Fe1.17), 4.8 mm (AlSi6.63Fe1.71) and 5.8 mm (AlSi4.62Fe1.23) as a first α-Al_8Fe_2Si phase may precipitate (before β-Al_5FeSi) in temperature range 612-614 ºC (white vertical ellipses on Fig. 11).

For the specimen AlSi7Fe1.0 (Fig. 12), Liquid mass fraction f_L and α-Al mass fraction f_α show the liquid channel wider and deeper than for AlSi5Fe1.0, and dendrites free area is 1 mm wide in the bottom at 577 ºC and 4 mm on top at 610 ºC. The mushy zone is shorter than for AlSi5Fe1.0, temperature range is about 575-615 ºC (13 mm long) for α-Al and 575-600 ºC for β-Al_5FeSi. The completely solidified microstructure in the center is also richer in β-Al_5FeSi (mass fraction about f_β=0.07). β-Al_5FeSi mass fraction f_β=0.02 reaches the temperature 600 ºC, and area in the center enriched in β-Al_5FeSi specimen appear parallel to liquid channel. By the shorter mushy zone (α-Al and Liquid mass fraction) and only slightly shorter β-Al_5FeSi growth range, in the center appeared the area (6 measurement points, Fig. 5-6) where β-Al_5FeSi precipitate before α-Al (Fig. 8).

Liquid mass fraction f_L and α-Al mass fraction f_α for AlSi7Fe0.5 (Fig. 13) are almost the same as for AlSi7Fe1.0, temperature range is about 575-615 ºC (13 mm long mushy) and dendrites free area is 1 mm wide in the bottom at 577 ºC and 4 mm on top at 610 ºC. The area of β-Al_5FeSi growth is very small, e.g. mass fraction 0.01 reaches temperature about 580 ºC and in only one selected point β-Al_5FeSi start to grow at about 585 ºC. β-Al_5FeSi mass fraction (about f_β=0.03) in temperature below 575 ºC is higher in the specimen center. High liquid mass fraction, low α-Al mass fraction and low β-Al_5FeSi mass fraction indicate high fluidity in the specimen center.

For the specimen AlSi9Fe0.2 (Fig. 14), Liquid mass fraction and α-Al mass fraction show the liquid channel, mushy zone temperature range is about 575-600 ºC (8.5 mm long mushy) and dendrites free area is 3 mm wide in the bottom at 575 ºC and 4 mm on top at 600 ºC. The higher Si content is clearly visible in comparison to previous specimens, so that α-Al mass fraction at 575 ºC reaches value about 0.3, whilst for specimen AlSi7Fe1.0 is 0.5. β-Al_5FeSi (Fig. 11c) start to precipitate at 575 ºC (about f_β=0.015 in the center), and liquid channel occur without this phase, so that formed widest and shallowest (575-600 ºC) liquid channel is completely empty of iron reach β phase.

The phase diagrams, Scheil-Gulliver solidification and property diagrams are the technique that is long time successfully used in materials science for description of complex relationship between composition, microstructure and process conditions. Described in current study application of property diagrams for mushy zone prediction is first and unique idea. On the 2D maps (Fig. 11-14) the most reliably are values of mass fraction for solidified area, at temperatures below 575 ºC. The view on mass fraction above 575 ºC is the projection resulting from chemical composition mostly frozen at 575 ºC, but real mushy zone is determined by Si and Fe release and intensive stirring (RMF) and can differ from Fig. 11-14.

The study on simulation of directional solidification for AlSi7 (G = 4 K/mm, B = 3 mT) by Hainke [16] take into consideration among other things solute release and fluid flow. The melt flow calculations [16] present velocity isolines that descent 4 mm in the specimen center in comparison to external part. The simulation results [16] showed liquid mass fraction isoline f_L=0.0 also reaching 4 mm deep into mushy in the central part of the specimen, and mass fraction isoline f_L=0.325 reached 7.15 mm. Current study presents comparable results to calculated by Hainke (without presence of β-Al_5FeSi), but clearly showing deeper liquid channel, 12-15 mm deep for specimen AlSi7Fe1.0 and 9-13 mm for AlSi7Fe0.5, with high liquid mass fraction and low α-Al mass fraction, and the presence of β phases.

The 2D maps showed the precipitation of β-Al_5FeSi before α-Al in liquid channel in AlSi5Fe1.0 and especially in AlSi7Fe1.0 specimen and the effect was earlier qualitatively described in [15]. From property diagram (Fig. 8) and 2D maps (Fig. 12) is known that about 50% of β-Al_5FeSi can precipitate before α-Al, and that happened for 6 points in area (liquid channel about 4 mm wide) about 2 mm wide (with final mass fraction f_β=0.07 below 575). Whilst in the rest of the area (about 6 mm wide) β-Al_5FeSi precipitates between dendrites or in eutectic reaction at 575 ºC. In this way it may be estimated, that about 33% of β precipitate before α-Al phase and can unbounded flow in the liquid melt.

Current results revealed precipitation of α–Al_8Fe_2Si phase in temperature range 614-612 ºC (Fig. 7 and white ellipse in the Fig. 11) before β-Al_5FeSi for AlSi5 Fe1.0 specimen. In two points it has appeared between dendrites, while in the third one in liquid channel where the phases might be carried out by stirring.

The 2D maps revealed mushy zone 18 mm long for AlSi5Fe1.0, 13 mm for AlSi7Fe1.0 and AlSi7Fe0.5, and 8.5 mm for AlSi9Fe0.2. The Si concentration means different fraction of AlSi eutectic and α-Al dendrites. For AlSi5Fe1.0 and AlSi7Fe1.0, 2D maps present liquid channel filled with β-Al_5FeSi, whilst for AlSi7Fe0.5 and AlSi9Fe0.2 it stay almost empty of β. This three factors strongly determine permeability of mushy zone in outer area and in the specimen center, and by generated magnetic field the occurred fluid flow should be analyzed carefully for each specimen. In the AlSi5Fe1.0 specimen, the fluid flow may be stronger damped by longer and denser dendritic structure and liquid channel filled with β-Al_5FeSi. However in AlSi9Fe0.2, the stirring of the alloy may be stronger because of mushy (shorter and thinner of α-Al) without β-Al_5FeSi (in wider liquid channel).

4. Conclusions

Property diagrams of phases mass fraction, based on the thermodynamic calculations and applied for building 2D maps seem to offer attractive method for visualizing mushy zone in directional solidification. Property diagrams and solidification paths (Scheil-Gulliver solidification) presented the segregation effect on the temperature and sequence of phases precipitation.

2D maps revealed liquid channel in center of the mushy zone, that can reach deep into mushy zone till final solidification reaction at temperature 575 ºC. The calculations presented the spatial location and mass fraction of phases (Liquid, α-Al, β-Al_5FeSi) in the mushy zone.

The study confirmed the qualitative results [15] showing precipitation of β-Al_5FeSi phase before the formation α-Al dendrites in the specimen center. Based on 2D maps, it was estimated that about 33% of all β-Al_5FeSi phases precipitated in the liquid channel, and possibly can flow (because of magnetic stirring) into liquid melt just above mushy zone. Current results revealed local precipitation of α–Al_8Fe_2Si (before β-Al_5FeSi).

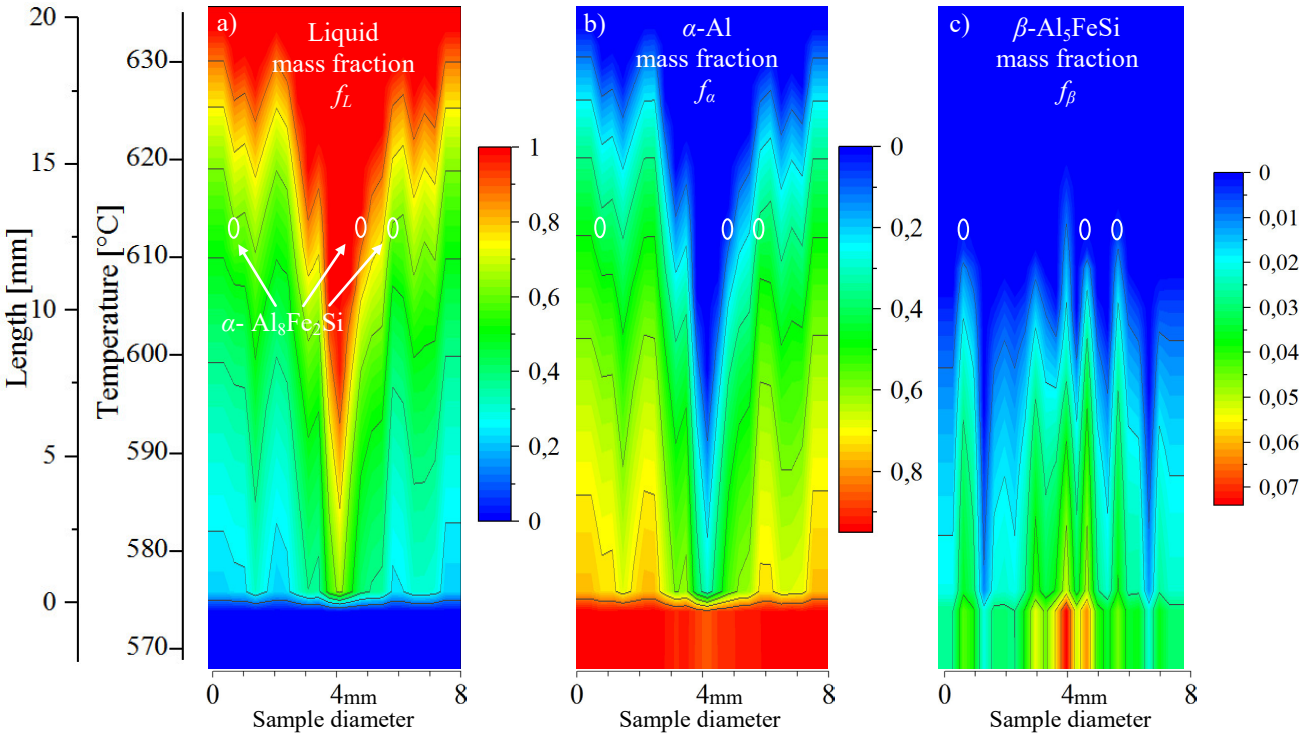

Fig. 11. 2D maps of mushy zone for AlSi5Fe1.0 specimen: a) Liquid mass fraction f_L, b) α-Al mass fraction f_α, c) β-Al_5FeSi mass fraction f_β in function of sample diameter and temperature/sample length

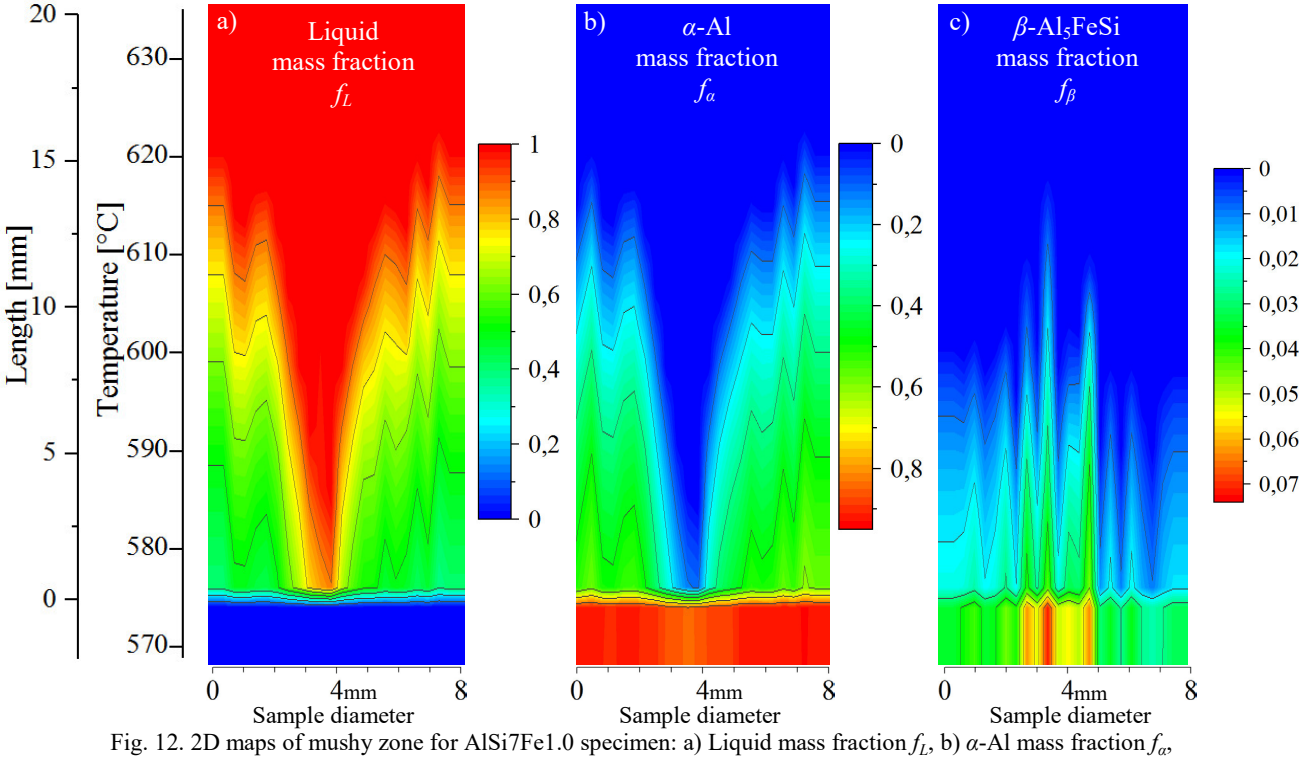

Fig. 12. 2D maps of mushy zone for AlSi7Fe1.0 specimen: a) Liquid mass fraction f_L, b) α-Al mass fraction f_α, c) β-Al_5FeSi mass fraction f_β in function of sample diameter and temperature/sample length

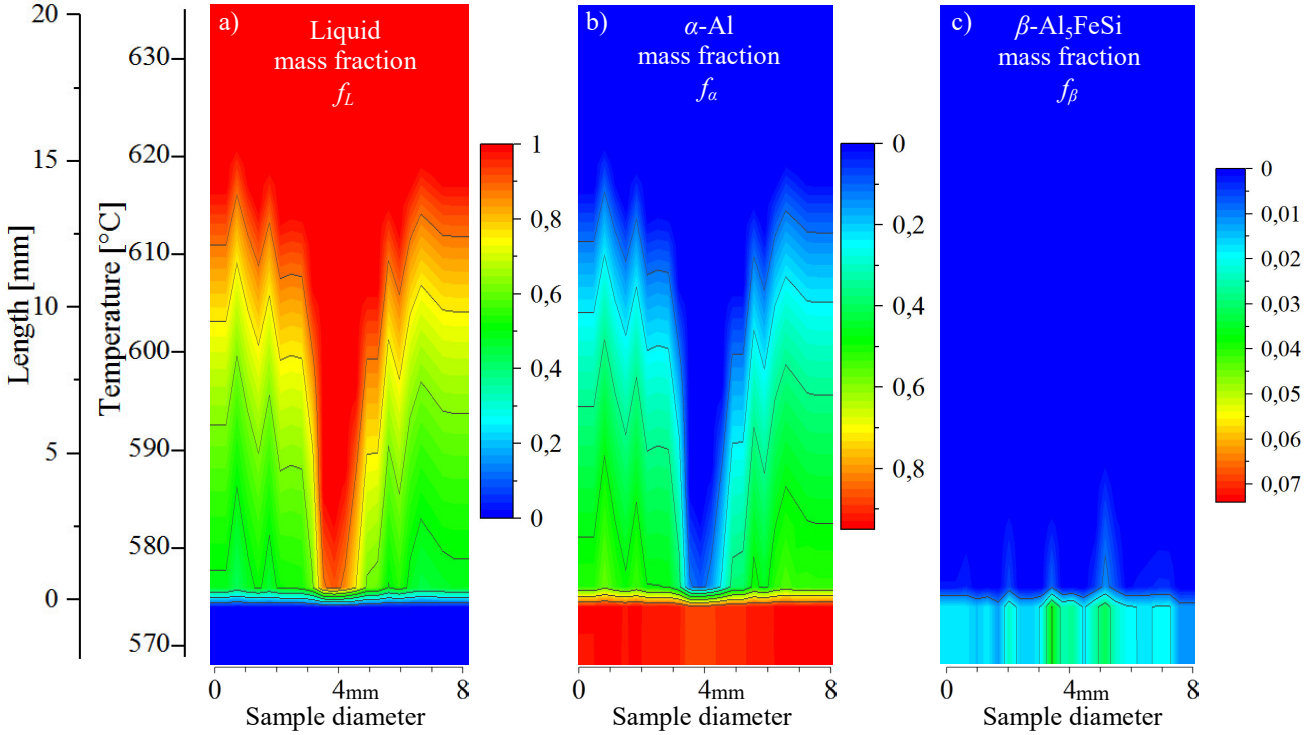

Fig. 13. 2D maps of mushy zone for AlSi7Fe0.5 specimen: a) Liquid mass fraction f_L, b) α-Al mass fraction f_α, c) β-Al$_5$FeSi mass fraction f_β in function of sample diameter and temperature/sample length

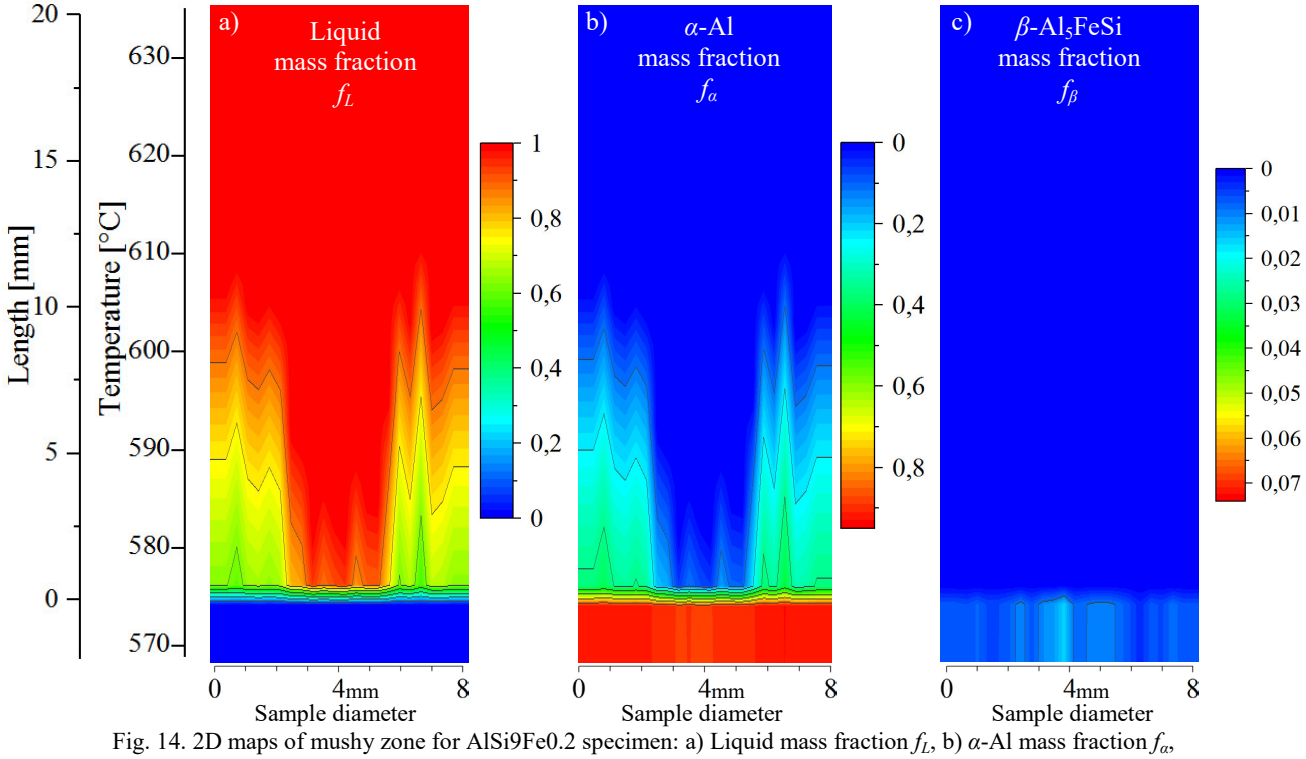

Fig. 14. 2D maps of mushy zone for AlSi9Fe0.2 specimen: a) Liquid mass fraction f_L, b) α-Al mass fraction f_α, c) β-Al$_5$FeSi mass fraction f_β in function of sample diameter and temperature/sample length

The found out liquid channel with β-Al_5FeSi shows high flow possibility of melt only and melt with Fe phase and the potential influence on the microstructure. Different flow possibilities in dendritic and eutectic area impose detailed analysis of the effect of fluid flow on the microstructure of each studied specimen alloy.

Acknowledgements

The research leading to these results has received funding from the People Programme (Marie Curie Actions) of the European Union's Seventh Framework Programme (FP7/2007-2013) under REA grant agreement n° PCIG13-GA-2013-613906.

References

[1] Massalski, T.B., Okamoto, H. (1990). Binary alloy phase diagrams. Materials Park, Ohio, ASM International, 1990. ISBN-13: 978-0871704030.

[2] Kaufman, L., Bernstein, H. (1970). Computer Calculation of Phase Diagrams with Special Reference to Refractory Metals. Academic Press, New York, NY, 1970.

[3] Lukas, H., Fries, S.G., Sundman, B. (2007). Computational Thermodynamics – The Calphad Method. Cambridge University Press 2007. ISBN 978-0-521-86811.

[4] Hillert, M. (1998). Phase Equilibria, Phase Diagrams and Phase Transformations – Their Thermodynamic Basis. Cambridge University Press 1998. ISBN 978-0-521-85351-4.

[5] Shi, P., Sundman, B. (2013). Thermo-Calc Software System – Thermodynamic Framework and Data. Thermo-Calc Software AB.

[6] Junga, H., Mangelinck-Noëlb, N., Nguyen-Thi, N. & Billia, B. (2009). Columnar to equiaxed transition during directional solidification in refined Al-based alloys. *Journal of Alloys and Compounds*, *Vol. 484, Issue 1-2*, 739–746. DOI: dx.doi.org/10.1016/j.jallcom.2009.05.029.

[7] Ruvalcaba, D., Mathiesen, R.H., Eskin, D.G., Arnberg, L. & Katgerman, L. (2007). In situ observations of dendritic fragmentation due to local solute-enrichment during directional solidification of an aluminum alloy. *Acta Materialia*, *Vol. 55, Issue 13*, 4287–4292. DOI: dx.doi.org/10.1016/j.actamat.2007.03.030.

[8] Tomaszewski, P.E. (2002). Jan Czochralski - Father of the Czochralski method. *Journal of Crystal Growth 236*, 1–4. DOI: dx.doi.org/10.1016/S0022-0248(01)02195-9.

[9] Duffar, T., Serrano, M.D., Moore, C.D., Camassel, J., Contreras, S. & Tanner, B.K. (1998). Bridgman solidification of GaSb in space. *Journal of Crystal Growth 192*, 63-72. DOI:dx.doi.org/10.1016/S0022-0248(98)00421-7.

[10] Alkemper, J., Sous, S., Stoker, C. & Ratke L. (1998). Directional solidification in an aerogel furnace with high resolution optical temperature measurements. *Journal of Crystal Growth 191*, 252-260. DOI: dx.doi.org/10.1016/S0022-0248(98)00114-6.

[11] Steinbach, S., Ratke, L. (2004). In situ optical determination of fraction solid. *Scripta Materialia 50*, 1135–1138. DOI: dx.doi.org/10.1016/j.scriptamat.2004.01.023.

[12] Steinbach, S. (2005). The influence of fluid flow on the microstructure evolution of directional solidified Al-Si and Al-Si-Mg alloys (in German). *Ph.D. Thesis*. RWTH, Germany.

[13] Thermo-Calc 4.1 – Software package from Thermo-Calc Software AB. Stockholm, Sweden. www.thermocalc.se.

[14] Mikolajczak, P. & Ratke, L. (2013). Effect of stirring induced by rotating magnetic field on beta-Al5FeSi intermetallic phases during directional solidification in AlSi alloys. *Int. J. Cast Met. Res.*, *vol. 26*, 339-353. DOI: dx.doi.org/10.1179/1743133613Y.0000000069.

[15] Mikolajczak, P. & Ratke, L. (2015). Interplay Between Melt Flow and the 3D Distribution and Morphology of Fe-Rich Phases in AlSi Alloys. *Metall. Mater. Trans. A, vol. 46A*, 1312—1327. DOI: dx.doi.org/10.1007/s11661-014-2692-4.

[16] Hainke, M. (2004). Computation of Convection and Alloys Solidification with the Software Package CrysVUn. *Ph.D. Thesis,* Technical Faculty Erlangen-Nuremberg, Germany.